International Journal of Power Electronics and Drive System (IJPEDS)
Vol. 17, No. 2, June 2026, pp. 1451~1461
ISSN: 2088-8694, DOI: 10.11591/ijpeds.v17.i2.pp1451-1461

Stability analysis of photovoltaic grid-connected power systems employing virtual synchronous generator control

Abdallah El Ghaly, Abdullah Hamdan, Mohamad Tarnini
Department of Electrical and Computer Engineering, Faculty of Engineering, Beirut Arab University, Beirut, Lebanon

Article Info

Article history:

Received Oct 6, 2025
Revised Apr 16, 2026
Accepted Apr 28, 2026

Keywords:

Grid stability
Grid-following control
Grid-forming control
Photovoltaic system
Power quality
Virtual synchronous generator
synchronous reference frame

ABSTRACT

The rapid integration of photovoltaic (PV) systems into power networks poses significant challenges to grid stability, including reduced inertia, voltage fluctuations, and limited fault ride-through (FRT) capabilities. This study presents a comparative analysis of two inverter control strategies: the synchronous reference frame (SRF) controller and the virtual synchronous generator (VSG) controller. A high-fidelity MATLAB/Simulink model was developed, incorporating the effects of irradiance and temperature, maximum power point tracking (MPPT), and battery energy storage system (BESS) interaction. Standardized fault scenarios were applied at PV penetration levels ranging from 30% to 150% in accordance with IEEE-1547, IEEE-519, and IEC 61727 requirements. The results show that SRF control achieves superior harmonic suppression, with a total harmonic distortion (THD) consistently below 0.5%, confirming its suitability for strong grids prioritizing power quality. However, its stability deteriorated at higher penetration levels, with the voltage overshoot reaching approximately 16% and recovery times exceeding 3 s. In contrast, the VSG control demonstrates enhanced transient stability and effective FRT performance, with the overshoot limited to ≤5% and recovery achieved within 0.8 s across all operating conditions. The main contribution of this study lies in the direct benchmarking of the SRF and VSG control strategies under identical operating conditions using a unified evaluation framework, including an extended analysis beyond 100% PV penetration. The findings highlight a fundamental trade-off between harmonic performance and transient stability and provide practical guidance for selecting appropriate inverter control strategies for renewable-dominated power systems.

Corresponding Author:

Mohamad Tarnini
Department of Electrical and Computer Engineering, Faculty of Engineering, Beirut Arab University
Beirut 11-5020, Lebanon
Email: m.tarnini@bau.edu.lb

1. INTRODUCTION

The advancement of photovoltaic (PV) technology is central to sustainable energy strategies, driven by climate change mitigation and the need to reduce greenhouse gas emissions [1]. The global PV capacity exceeded 1 TW in 2022 and is projected to supply more than 30% of the electricity demand by 2050, supported by declining costs, efficiency gains, and favorable policies [2]. Despite this growth, the intermittency of solar irradiance and lack of inherent inertia challenge grid reliability and stability [3], [4].

Conventional grids rely on synchronous generators for inertia, frequency regulation, and fault-ride-through (FRT). However, PV inverters act as grid-connected voltage sources without physical inertia, which can increase the rate of change of frequency (RoCoF), voltage instability, and harmonic distortion in weak

grids [5]–[7]. To address these issues, grid codes such as IEEE-1547, IEEE-519, IEC 61727, and ENTSO-E mandate low-voltage ride-through (LVRT), harmonic suppression, and reactive current support [8].

Among the control methods, the synchronous reference frame (SRF) controller, a grid-following approach, offers accurate active/reactive power control and excellent harmonic suppression [9], [10]. However, its reliance on phase-locked loops (PLLs) renders it less robust in weak grids [11], [12]. In contrast, the virtual synchronous generator (VSG), a grid-forming approach, emulates synchronous machine inertia and damping, thereby improving the transient response and frequency stability [13], [14]. However, it is more sensitive to parameter tuning and is generally inferior in terms of harmonic suppression [15], [16].

Recent studies reflect these trade-offs: SRF improves harmonic suppression and transient control [12], [13], whereas adaptive VSGs enhance fault ride-through and inertia support [17]–[20]. However, VSG performance is highly dependent on the inertia and damping coefficients [21], [22], and comparative evaluations remain scarce, often assessing the SRF for power quality and VSG for stability under different conditions [23].

Despite these advancements, several limitations remain in the field. Many existing studies adopt simplified DC-link representations or ideal DC sources, neglecting the influence of photovoltaic operating conditions, such as irradiance and temperature, on system performance. In addition, comparative analyses between the SRF and VSG controllers are often conducted under non-uniform operating conditions, limiting the validity of the conclusions. Furthermore, comprehensive evaluations under short-circuit fault scenarios are limited, particularly those using standardized performance metrics such as recovery time, RoCoF, and fault ride-through capability. This limits the ability to assess realistic grid behavior under disturbance conditions in the field.

This study addresses these gaps by i) Developing a PV model incorporating irradiance and temperature effects with maximum power point tracking (MPPT); ii) Integrating a battery energy storage system (BESS) for coordinated control; and iii) Conducting a systematic fault-based evaluation across PV penetration levels ranging from 30% to 150%. Unlike prior studies with simplified models or non-standard test conditions, this study employs IEEE/IEC-aligned benchmarking metrics, including total harmonic distortion (THD), recovery time, and FRT compliance, with stress scenarios up to 150% penetration to emulate over-generation conditions.

The contribution of this study stems from assessing the SRF and VSG control strategies under the same operating conditions within a unified benchmarking framework. The results show that SRF control is better suited for strong grids where high power quality is essential, while VSG control demonstrates greater robustness in weak or low-inertia systems. These findings provide practical guidance for the design and operation of stable PV-dominated power systems across a range of grid conditions.

2. METHOD

This study employs a MATLAB/Simulink-based simulation framework to evaluate and compare the performance of SRF and VSG control strategies for grid-connected PV systems. The analysis was conducted under identical operating and disturbance conditions to ensure a fair and consistent comparison in accordance with the IEEE/IEC requirements.

2.1. System overview

The simulated system consisted of a grid-connected PV generation unit interfaced through a DC–DC boost converter and a voltage source inverter (VSI), which was connected to the grid via an LCL filter at the point of common coupling (PCC). The PV array operates under fixed environmental conditions with irradiance set to 1000 W/m² and temperature maintained at 25 °C. MPPT was implemented using the perturb and observe (P&O) algorithm. A battery energy storage system (BESS) rated at 60 kW was integrated on the DC side to support the transient power exchange during disturbances.

In this study, the PV generation was maintained constant at 36 kW for all simulation scenarios. The PV penetration level is defined by varying the load demand while keeping the PV output constant. This approach enables a controlled evaluation of the system performance across penetration levels ranging from 30% to 150%, ensuring that variations in the system behavior are attributed to the loading conditions rather than changes in generation.

The simulation was performed in a discrete environment using a fixed-step solver with a sampling time of 10 µs, allowing an accurate representation of the switching dynamics and control responses. The total simulation duration was 5 s, covering the pre-fault, fault, and post-fault operating intervals. The overall configuration of the grid-connected PV system is shown in Figure 1, and the SRF and VSG control implementations are illustrated in Figure 2. The main electrical and control parameters used in the simulation are listed in Table 1. Measurement blocks are implemented at the PCC to record system variables, including voltage, current, THD, voltage deviations, and transient response indicators used in the performance evaluation.

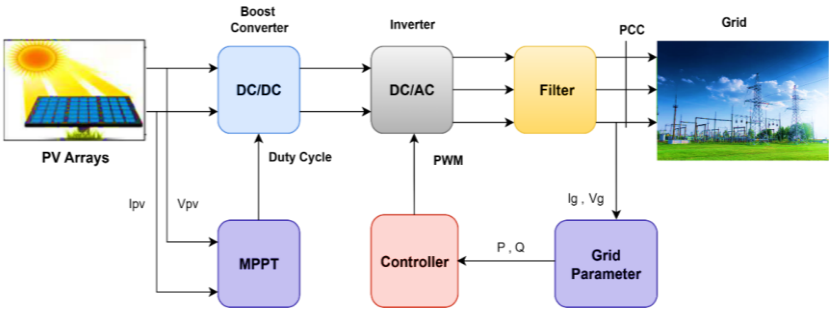

Figure 1. General model of the grid-connected PV system

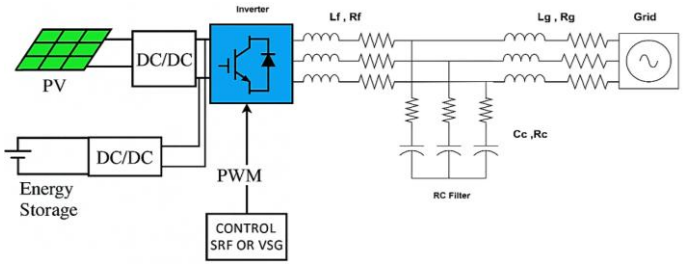

Figure 2. Model of the grid-connected PV system with SRF/VSG control configurations

Table 1. System parameters for SRF and VSG control implementation

Parameter	Symbol	Value	Parameter	Symbol	Value
Rf (inverter side)	Rf	0.1 Ω	DC-link voltage	Vdc	800 V
Lf (inverter side)	Lf	5 mH	Rc– filter branch	Rc	0.5 Ω
Rg (grid side)	Rg	0.03 Ω	Cc – filter branch	Cc	40 µF
Lg (grid side)	Lg	0.35 mH	J (VSG inertia constant)	J	0.5 s
Frequency	f	50 Hz	D (VSG damping factor)	D	10 pu·s
Grid voltage (L-L RMS)	V grid	380 V			

2.2. Synchronous reference frame (SRF) control

The SRF controller is a widely adopted grid-following method that regulates active and reactive currents by synchronizing with the grid using a PLL. In the dq rotating frame, proportional–integral (PI) regulators independently control the current components, enabling accurate power regulation and robust harmonic suppression [24]. This structure is well-suited for stiff grids but exhibits reduced robustness under weak-grid conditions owing to its reliance on the PLL. The general control scheme is illustrated in Figure 3. Although the SRF controller provides a reliable benchmark for harmonic performance, it lacks the capability to emulate physical inertia or damping. This limitation motivates the use of VSG control, which is described in the following subsection as the main focus of this study.

2.3. Virtual synchronous generator (VSG) control

The VSG controller is a grid-forming strategy that emulates synchronous generator dynamics by introducing virtual inertia and damping effects. The simplified control structure is shown in Figure 4. Its behavior is governed by the swing in (1) [25].

$$\begin{cases} J\frac{d\omega}{dt} = T_m - T_e - D\Delta\omega = \frac{P_m}{\omega} - \frac{P}{\omega} - D(\omega - \omega_0) \\ \frac{d\delta}{dt} = \omega - \omega_0 \end{cases} \quad (1)$$

In this context, ω and ω_0 represent the instantaneous angular speed and nominal frequency of the grid, respectively. T_m and T_e correspond to the mechanical torque and electromagnetic torque, while P_m and P denote the mechanical input power and electrical output power, respectively. J refers to the moment of inertia, D is the damping factor, and δ represents the power angle. To emulate the primary frequency regulation behavior of a conventional synchronous machine, prime mover control is incorporated into the VSG structure. The virtual prime mover control is described by (2).

$$P_m = P_{ref} + K_\omega(\omega_0 - \omega) \tag{2}$$

By substituting (2) into (1) and applying the Laplace transformation, the closed-loop frequency response is obtained as (3), where the equivalent time constant and droop coefficient are defined in (4), respectively.

$$\frac{\omega_0-\omega}{P_{ref}-P} = -\frac{1}{J\omega_0 s+D\omega_0+K_\omega} = -\frac{m_p}{\tau s+1} \tag{3}$$

$$\begin{cases} \tau = \frac{J\omega_0}{D\omega_0+K_\omega} \\ m_p = \frac{1}{D\omega_0+K_\omega} \end{cases} \tag{4}$$

As shown in (3) and (4), the inertia constant J and damping factor D govern the frequency dynamics of the system. A larger J provides stronger inertial support and limits the frequency deviation but slows the transient response, whereas a smaller J accelerates the dynamics yet risks instability if the damping is inadequate. The damping factor D controls the oscillations: higher values suppress the swings, whereas lower values may cause sustained oscillations. Improper tuning of J and D can destabilize the system; in practice, low inertia with optimized damping enables fast transients, whereas high inertia with added damping enhances robustness [26].

Voltage regulation is achieved via reactive power–voltage droop control as (5).

$$U_{ref} = U_N + m_Q\left(Q_{ref} - Q\right) \tag{5}$$

In (5), U_N and U_{ref} denote the rated and reference voltages, respectively. Q_{ref} represents the reference reactive power, while Q indicates the actual reactive power delivered by the system. The parameter Q_{ref} refers to the reactive power–voltage droop coefficient. This control mechanism enables decentralized voltage regulation by adjusting the inverter output voltage according to the reactive power demand. An appropriate choice of m_Q facilitates accurate reactive power sharing among multiple inverters and improves the overall voltage stability of the system. As shown in Figure 4, the VSG approach mimics synchronous machine dynamics, providing an inertial response, frequency stability, and robust fault ride-through. Its effectiveness depends strongly on the proper tuning of the inertia (J), damping (D), and droop coefficients.

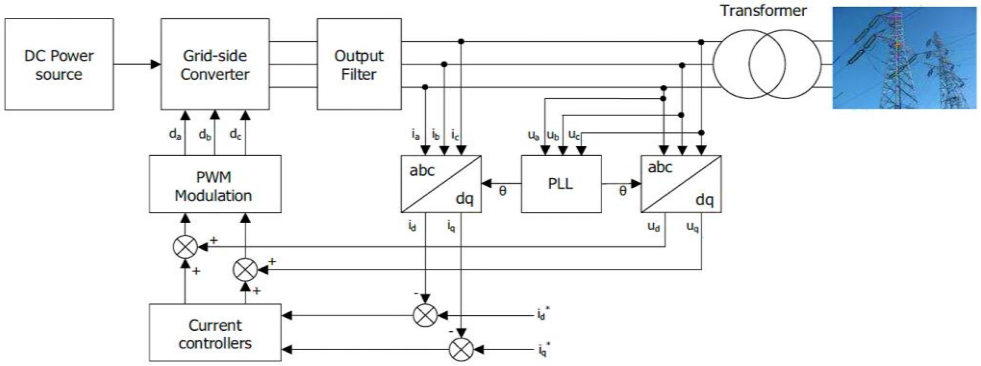

Figure 3. Control structure for synchronously rotating reference frame [24]

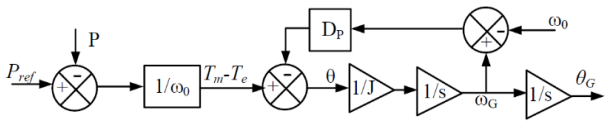

Figure 4. Simplified swing-based virtual synchronous generator

2.4. Simulation procedure

The system was initially operated under steady-state conditions at a specified irradiance and temperature. A three-phase short-circuit fault was then applied at the PCC for a duration of 0.2 s to represent a severe disturbance. Following fault clearance, the transient recovery behavior was recorded. The simulation

was repeated for PV penetration levels ranging from 30% to 150% by varying the load demand while maintaining constant PV generation. Identical system configurations and disturbance conditions were applied to both the SRF and VSG control strategies to ensure reproducibility and objective comparison.

2.5. Evaluation metrics

The performance of the control strategies was evaluated using a set of metrics that captured both power quality and dynamic stability. THD was used to assess the current quality. The voltage overshoot (%) and voltage surge (V) quantify the magnitude of transient voltage deviations during disturbances, whereas the transient recovery time (s) represents the time required for the system to return to a steady-state operation.

Frequency stability is evaluated using the rate of change of frequency (RoCoF) and frequency nadir, defined as the minimum frequency reached during a disturbance. In addition, the power angle (δ) was monitored to assess the system synchronism and overall stability. All measurements were obtained at the PCC using simulation monitoring tools, ensuring consistency and accuracy across all scenarios.

3. RESULTS AND DISCUSSION

This section evaluates the comparative performance of the SRF and VSG control strategies under PV penetration values changing from 30% to 150%, depending on the system model defined in Section 2. The analysis considered key performance indicators, including THD, voltage regulation (%VR), transient overshoot, recovery time, voltage surge, frequency dynamics, and power angle δ (rad).

The evaluation was conducted in accordance with the control strategies and performance characteristics reported in the literature [17], [20], [27], as well as international grid standards, including IEEE-1547 [28], IEEE-519 [29], and IEC 61727 [30]. Representative waveforms at 100% PV penetration are presented for both normal and faulted operating conditions, as shown in Figures 5–8. The system performance at lower (30%) and higher (125%–150%) penetration levels is summarized in Tables 2 and 3, and a comparative overview of all scenarios is provided in Figure 9. This unified evaluation under identical operating conditions enables a consistent assessment of the SRF and VSG performances and highlights their operational limits under increasing PV penetration.

3.1. Normal operation performance

Under steady-state conditions, both controllers maintained synchronism with the grid at all penetration levels. However, distinct differences were observed in the harmonic performance and voltage regulation, as illustrated in Figures 5 and 6 and summarized in Tables 2 and 3. The SRF controller (Figure 5 and Table 2) demonstrated excellent harmonic suppression, with the THD consistently below 0.5%, thereby satisfying the limits defined in IEEE-519 [29]. A slight overvoltage condition (%VR ≈ −1.5%) was observed at higher penetration levels, primarily because of the increased active power injection and dependence on PLL dynamics. The power angle δ remained stable at approximately 0.2 rad, indicating strong synchronism.

In contrast, the VSG controller (Figure 6 and Table 3) achieved tighter voltage regulation, with |%VR| not exceeding 1.81% across all penetration levels and remaining within approximately 1.5% for most operating points. The THD ranged between 1.14% and 1.76%, remaining within IEEE-519 compliance [29]. This behavior is attributed to droop-based voltage regulation and virtual inertia, which enhance power sharing and grid support. The power angle δ stabilized at approximately 0.25 rad, reflecting improved active power transfer capability.

These results confirm a clear trade-off between the two control strategies under steady state conditions. The SRF controller provides superior harmonic suppression because its current regulation is directly synchronized with the grid through the dq reference frame, whereas the VSG controller achieves tighter voltage support through droop-based regulation and virtual inertia. Accordingly, the SRF is more suitable when power quality is the dominant objective, whereas the VSG offers a stronger voltage support capability under varying operating conditions.

Table 2. Performance of SRF control under varying PV penetration levels during normal operation and post-SCC (0.2 s)

PV penetration level	PV (kW)	Load (kW)	PCC voltage normal	Grid voltage (V)	THD (%)	%VR normal	Voltage at PCC (V) post SCC	%VR post SCC	V surge post SCC	Transient time (s)	Overshoot (%)
30%	36.0	120.0	372.32	380	0.2	2.06	379.67	0.09	391.92	1.9	3
50%	36.0	72.0	377.22	380	0.23	0.74	389.47	2.49	395.59	2.2	4
70%	36.0	51.43	378.45	380	0.33	0.41	391.92	3.14	398.04	2.4	5
100%	36.0	36.0	385.79	380	0.4	-1.5	394.37	3.78	428.66	2.6	13
125%	36.0	28.8	380.9	380	0.34	-0.24	394.37	3.78	440.91	2.9	16
150%	36.0	24.0	382.12	380	0.36	-0.55	391.92	3.14	431.11	3.1	13

Table 3. Performance of VSG control under varying PV penetration levels during normal operation and post-SCC (0.2 s)

PV penetration level	PV (kW)	Load (kW)	PCC voltage normal	Grid voltage (V)	THD (%)	%VR normal	Voltage at PCC (V) post SCC	%VR post SCC	V surge post SCC	Transient time (s)	Overshoot (%)
30%	36.0	120.0	377.0	380	1.14	0.74	379.67	-0.09	379.67	0.7	0
50%	36.0	72.0	381.0	380	1.35	-0.24	385.79	1.52	391.92	0.8	3
70%	36.0	51.43	383.0	380	1.5	-0.87	387.02	1.85	396.82	0.8	4
100%	36.0	36.0	386.0	380	1.76	-1.5	388.24	2.17	399.27	0.8	5
125%	36.0	28.8	386.0	380	1.2	-1.5	388.24	2.17	388.24	0.6	2
150%	36.0	24.0	387.0	380	1.15	-1.81	387.02	1.85	389.47	0.6	2

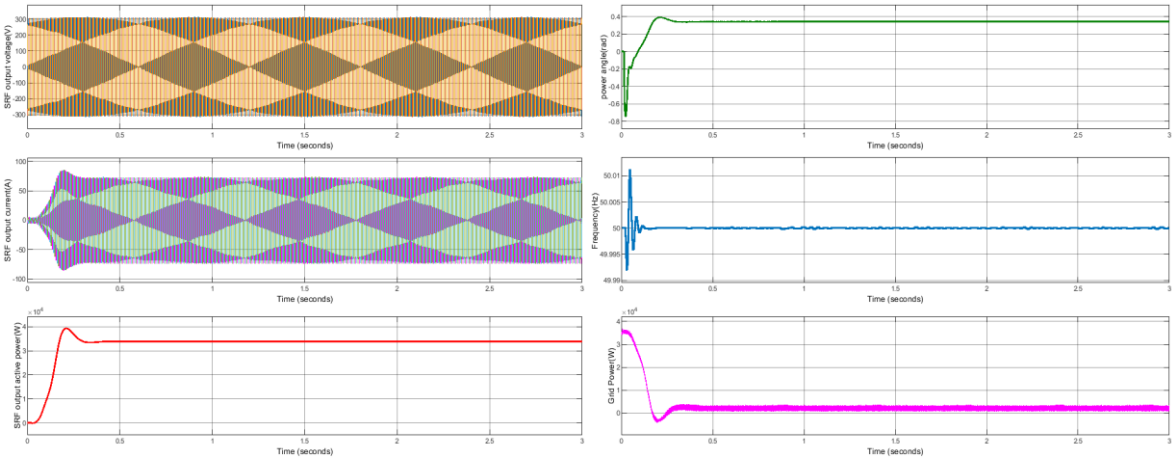

Figure 5. SRF control performance at 100% PV penetration during normal operation, showing the voltage, current, power, frequency response, and power angle δ

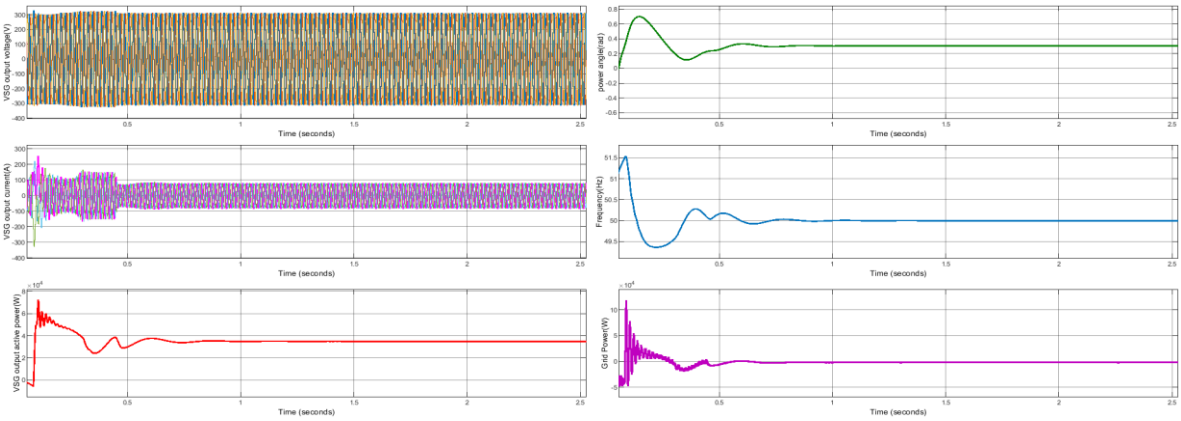

Figure 6. VSG controls performance at 100% PV penetration during normal operation, showing voltage, current, power, frequency response, and power angle δ

3.2. Fault ride-through and transient response

The transient performance of both controllers was evaluated under a 0.2 s three-phase short-circuit fault at the 100% PV penetration level, as illustrated in Figures 7 and 8 and summarized in Tables 2 and 3. The SRF controller (Figure 7 and Table 2) exhibited significant transient stress, with the voltage overshoot reaching approximately 13%, the surge voltage increasing to approximately 428.66 V, and the recovery time extending to approximately 2.6 s. The frequency dropped to approximately 49.7 Hz, accompanied by a high rate of change of frequency (RoCoF), whereas the power angle δ increased to approximately 0.9 rad before reconverging. This response indicates that the grid-following structure is more sensitive to severe faults because the synchronization depends on the PLL tracking of the disturbed grid voltage. Consequently, the

controller experiences larger transient excursions and slower post-fault recovery, consistent with the limitations reported in [15], [16], while also approaching or exceeding the limits defined in IEEE-1547 [28] and IEC 61727 [30].

In contrast, the VSG controller (Figure 8 and Table 3) demonstrated superior transient performance, with the overshoot limited to ≤5% and recovery achieved within 0.8 s. The frequency nadir remained close to the nominal value of approximately 49.85 Hz, and the power angle δ exhibited well-damped oscillations throughout the post-fault interval. This improved behavior arises from the virtual inertia and damping embedded in the VSG structure, which moderate the frequency deviation, reduce oscillatory behavior, and support faster restoration of voltage and synchronism after fault clearance. These findings are consistent with previous studies on VSG-based control strategies [17], [20], [27].

3.3. High penetration analysis (125–150%)

To assess the system robustness under extreme operating conditions, the analysis was extended to PV penetration levels of 125%–150%, as summarized in Tables 2 and 3, and illustrated in Figure 9. The SRF controller (Table 2 and Figure 9) exhibited noticeable performance degradation at high penetration levels. The voltage overshoot reached 16% at 125% penetration, whereas the transient recovery time increased to 3.1 s at 150% penetration.

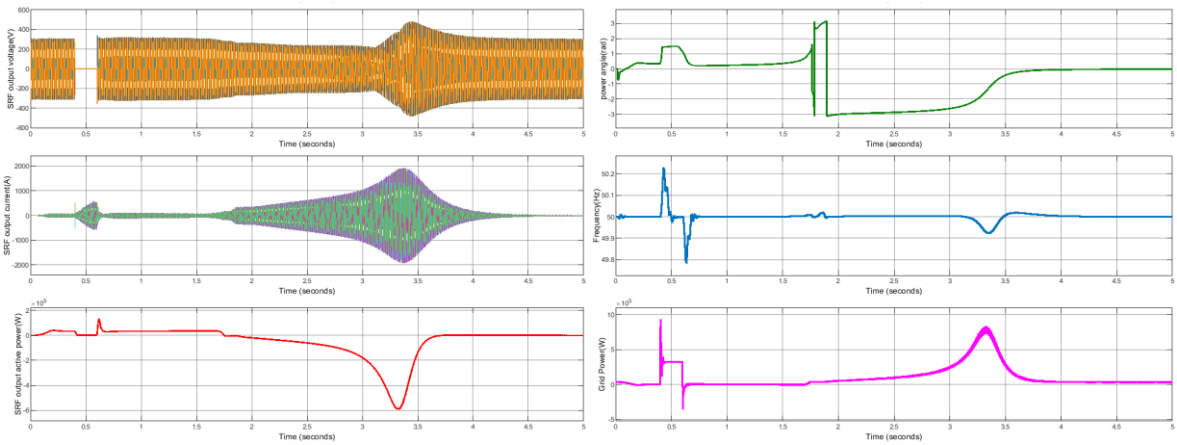

Figure 7. SRF control performance at 100% PV penetration during a 0.2-s fault, showing voltage, current, active power, frequency response, and power angle δ

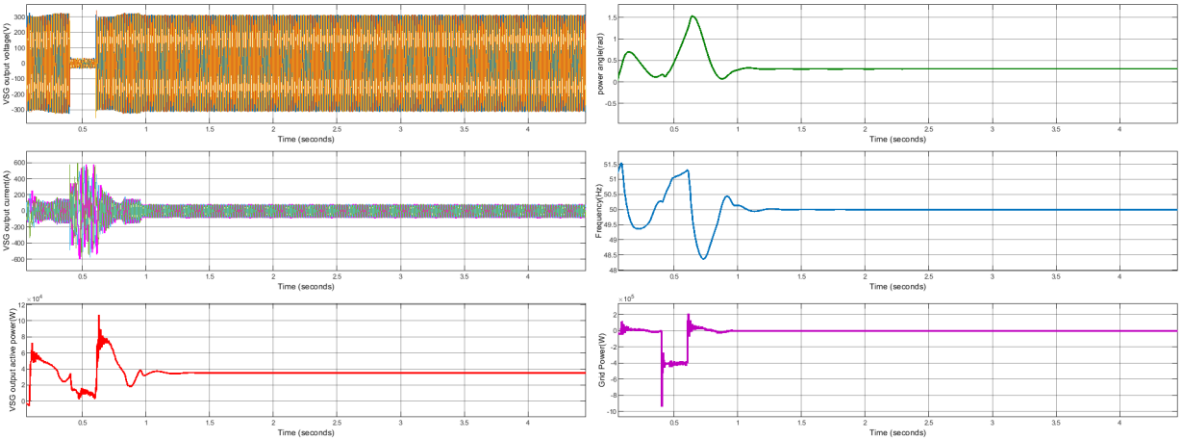

Figure 8. VSG controls performance at 100% PV penetration during a 0.2-s fault, showing voltage, current, active power, frequency response, and power angle δ

In addition, the surge voltage increased to 440.91 V at 125% penetration and remained high at 431.11 V at 150% penetration, exceeding the acceptable limits defined in IEEE-1547 [28] and IEC 61727 [30]. The power angle δ approached 1 rad, indicating weakened synchronism and a reduced stability margin

under highly stressed operating conditions. In contrast, the VSG controller (Table 3 and Figure 9) maintained stable operation across the same high penetration range. The overshoot remained limited to 2%, the recovery time was reduced to 0.6 s, and the surge voltage remained within the relatively narrow range of 388.24–389.47 V. The frequency nadir remained above 49.8 Hz, and the oscillations of the power angle δ were well-damped, confirming strong synchronism and superior dynamic stability.

These results demonstrate that the VSG controller provides substantially greater robustness than the SRF controller under overgeneration and high-penetration conditions. In particular, the contrast becomes more pronounced above 100% penetration, where the SRF controller shows clear degradation in the overshoot, surge voltage, and recovery time, whereas the VSG controller preserves a stable and well-damped behavior. This extended analysis up to 150% penetration strengthens the practical relevance of the study by revealing the operating limits of both strategies under stressed conditions, which are not commonly examined in direct comparative studies.

3.4. Comparison with the state of the Art

The performance trends across all PV penetration levels are summarized in Tables 2 and 3 and illustrated in Figure 9. The SRF controller (Table 2 and Figure 9) consistently achieved low THD values below 0.5%, confirming its suitability for applications that prioritize power quality and remain well within the limits specified by the IEEE-519 [29]. This observation is consistent with previous studies that reported the strong harmonic suppression capability of SRF-based control strategies [12], [13]. However, under higher penetration levels, the SRF controller exhibits degraded transient performance, including increased overshoot, longer recovery time, and weakened synchronism, primarily because of its reliance on phase-locked loop synchronization, as discussed in [15], [16].

In contrast, the VSG controller (Table 3 and Figure 9) exhibited slightly higher THD values, ranging from 1.14% to 1.76%, but still remained within the IEEE-519 compliance [29]. Simultaneously, it provides clearly superior transient performance, including lower overshoot, faster recovery, and improved frequency stability across all operating conditions. These findings are consistent with earlier studies highlighting the advantages of grid-forming control strategies in low-inertia and disturbance-prone systems [17]–[20], [27].

Compared with most previous studies, this study provides a direct and controlled benchmark between the SRF and VSG controls under identical operating conditions using a unified evaluation framework. Its main contribution is the systematic comparison of grid-following and grid-forming strategies across a wide penetration range, including stressed overgeneration scenarios up to 150%. The results show that the relative advantage of each controller depends strongly on the selected performance objective: the SRF remains preferable when a low THD is required, whereas the VSG becomes more advantageous when transient stability, damping, and fault ride-through are prioritized.

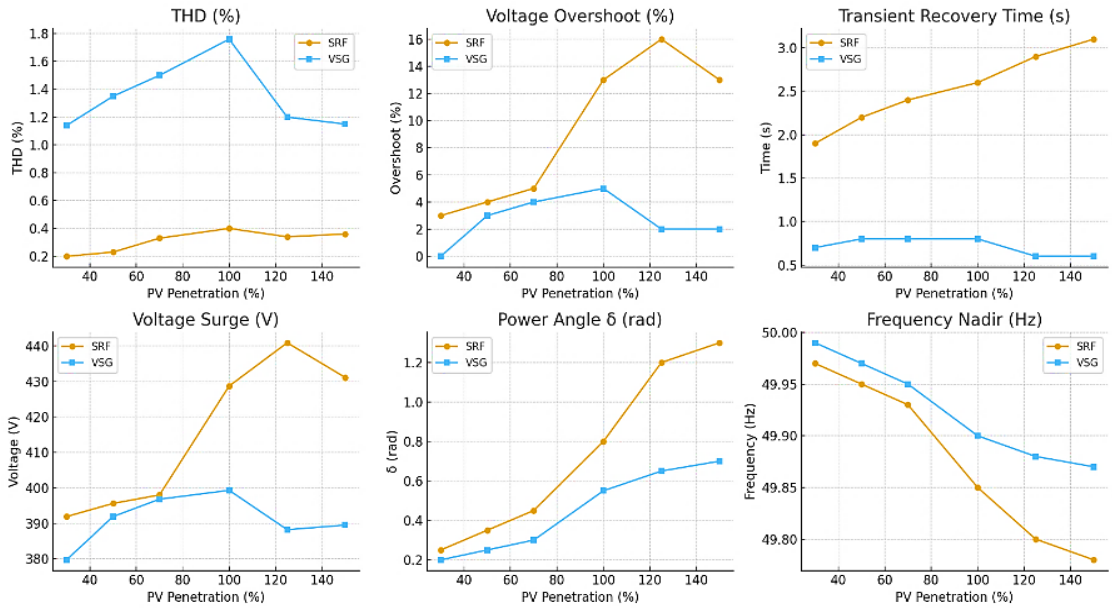

Figure 9. Comparative performance of SRF and VSG controllers at different PV penetration levels (30–150%) based on key power quality and stability metrics

3.5. Implications of the results

The results provide practical guidance for selecting inverter control strategies in modern power systems. The SRF controller remains attractive for applications in which harmonic suppression and accurate steady-state current regulation are the primary requirements. However, its reduced robustness during faults and at high penetration levels indicates that its performance margin becomes narrower as the operating conditions become more stressed. In contrast, the VSG controller offers stronger transient stability, improved damping, and superior fault ride-through capability, making it a more suitable option when dynamic support and post-fault recovery are the dominant design priorities. These results further indicate that hybrid or adaptive control approaches, which integrate the superior harmonic performance of the SRF with the inertial support capability of the VSG, could represent a promising solution for the development of future inverter-dominated power systems.

3.6. Limitations and future work

This study is based on MATLAB/Simulink simulations, without experimental validation. The battery energy storage system was represented in an idealized manner, and the analysis focused on symmetrical fault scenarios. Future work will include experimental or hardware-in-the-loop validation, investigation of unbalanced fault conditions, and integration of advanced energy storage modeling and hybrid control strategies to further enhance system performance.

4. CONCLUSION

In this study, a high-fidelity MATLAB/Simulink model was developed to evaluate the stability of grid-connected PV power systems under varying penetration scenarios. The study integrated a PV array model incorporating irradiance and temperature effects, together with MPPT and a coordinated battery energy storage system (BESS). Within this unified framework, the performances of SRF and VSG control strategies were evaluated under standardized fault scenarios at penetration levels ranging from 30% to 150%, with the performance assessed relative to the IEEE-1547, IEEE-519, and IEC 61727 requirements.

The results revealed a fundamental trade-off between the power quality and transient stability of inverter-dominated grids. The SRF controller demonstrated superior harmonic suppression, maintaining the THD consistently below 0.5%, which makes it well-suited for strong grids where power quality is a primary requirement. However, its stability deteriorated significantly at high penetration levels, with the voltage overshoot reaching approximately 16% and recovery times exceeding 3 s. In contrast, the VSG controller provided enhanced resilience through virtual inertia and damping, limiting the voltage overshoot to ≤5% and achieving fault recovery within 0.8 s across all operating conditions.

The main contribution of this study lies in the direct benchmarking of grid-following and grid-forming control strategies under identical operating conditions using a unified evaluation framework, with the analysis extended to over-generation conditions up to 150% penetration. This study clarifies the performance boundaries of SRF and VSG control under common test conditions and standardized performance indicators. The findings provide practical guidance for grid operators and system designers, showing that SRF control is more suitable when power quality is the primary concern, whereas VSG control offers clear advantages in terms of transient stability and fault ride-through under stressed operating conditions.

Despite these contributions, the study remains limited by its simulation-based nature and use of an idealized energy-storage representation. Future work will focus on experimental or hardware-in-the-loop validation, investigation of unbalanced fault conditions, and development of hybrid control strategies that combine the harmonic performance of SRF with the inertial support of VSG. These developments are expected to further improve the stability and reliability of next-generation power systems.

FUNDING INFORMATION

Authors state no funding involved.

AUTHOR CONTRIBUTIONS STATEMENT

This journal uses the Contributor Roles Taxonomy (CRediT) to recognize individual author contributions, reduce authorship disputes, and facilitate collaboration.

Name of Author	C	M	So	Va	Fo	I	R	D	O	E	Vi	Su	P	Fu
Abdallah El Ghaly	✓	✓	✓	✓	✓	✓		✓	✓	✓	✓	✓	✓	
Abdullah Hamdan		✓	✓			✓		✓	✓	✓	✓			✓
Mohamad Tarnini	✓		✓	✓			✓			✓	✓	✓	✓	

C : **C**onceptualization
M : **M**ethodology
So : **So**ftware
Va : **Va**lidation
Fo : **Fo**rmal analysis
I : **I**nvestigation
R : **R**esources
D : **D**ata Curation
O : Writing - **O**riginal Draft
E : Writing - Review & **E**diting
Vi : **Vi**sualization
Su : **Su**pervision
P : **P**roject administration
Fu : **Fu**nding acquisition

CONFLICT OF INTEREST STATEMENT

The authors declare no conflicts of interest.

DATA AVAILABILITY

The data that support the findings of this study are available from the corresponding author [MT], upon reasonable request.

REFERENCES

[1] S. A. Awuku, F. Muhammad-Sukki, and N. Sellami, "Building integrated photovoltaics—the journey so far and future," *Energies*, vol. 15, no. 5, p. 1802, Feb. 2022, doi: 10.3390/en15051802.

[2] W. Zhang, Y. Zhao, F. Huang, Y. Zhong, and J. Zhou, "Forecasting the energy and economic benefits of photovoltaic technology in china's rural areas," *Sustainability*, vol. 13, no. 15, p. 8408, Jul. 2021, doi: 10.3390/su13158408.

[3] F. Czepło and P. F. Borowski, "Innovation solution in photovoltaic sector," *Energies*, vol. 17, no. 1, p. 265, Jan. 2024, doi: 10.3390/en17010265.

[4] J. Zhang, P. Zhao, Z. Zhang, Y. Yang, F. Blaabjerg, and Z. Dai, "Fast amplitude estimation for low-voltage ride-through operation of single-phase systems," *IEEE Access*, vol. 8, pp. 8477–8484, 2020, doi: 10.1109/ACCESS.2019.2963226.

[5] A. Zdyb and S. Gulkowski, "Performance assessment of four different photovoltaic technologies in Poland," *Energies*, vol. 13, no. 1, p. 196, Jan. 2020, doi: 10.3390/en13010196.

[6] C. Chi, H. Zhao, and J. Han, "Study on quantitative evaluation index of power system frequency response capability," *Energies*, vol. 15, no. 24, p. 9423, Dec. 2022, doi: 10.3390/en15249423.

[7] W. Yuan, X. Yuan, L. Xu, C. Zhang, and X. Ma, "Harmonic loss analysis of low-voltage distribution network integrated with distributed photovoltaic," *Sustainability*, vol. 15, no. 5, p. 4334, Feb. 2023, doi: 10.3390/su15054334.

[8] N. Mansouri, A. Lashab, J. M. Guerrero, and A. Cherif, "Photovoltaic power plants in electrical distribution networks: a review on their impact and solutions," *IET Renewable Power Generation*, vol. 14, no. 12, pp. 2114–2125, Sep. 2020, doi: 10.1049/iet-rpg.2019.1172.

[9] G. M. El-Banby, N. M. Moawad, B. A. Abouzalm, W. F. Abouzaid, and E. A. Ramadan, "Photovoltaic system fault detection techniques: a review," *Neural Computing and Applications*, vol. 35, no. 35, pp. 24829–24842, Dec. 2023, doi: 10.1007/s00521-023-09041-7.

[10] A. Q. Al-Shetwi, M. A. Hannan, K. P. Jern, A. A. Alkahtani, and A. E. PG Abas, "Power quality assessment of grid-connected PV system in compliance with the recent integration requirements," *Electronics*, vol. 9, no. 2, 2020, doi: 10.3390/electronics9020366.

[11] X. Wang, M. G. Taul, H. Wu, Y. Liao, F. Blaabjerg, and L. Harnefors, "Grid-synchronization stability of converter-based resources—an overview," *IEEE Open Journal of Industry Applications*, vol. 1, pp. 115–134, 2020, doi: 10.1109/OJIA.2020.3020392.

[12] G. I. Orfanoudakis, E. Koutroulis, G. Foteinopoulos, and W. Wu, "Synchronous reference frame current control of Aalborg-type PV inverters," in *2021 23rd European Conference on Power Electronics and Applications (EPE'21 ECCE Europe)*, Sep. 2021, p. P.1-P.10, doi: 10.23919/EPE21ECCEEurope50061.2021.9570425.

[13] M. Li, Y. Gui, Z. Jin, Y. Guan, and J. M. Guerrero, "A synchronous-reference-frame I-V droop control method for parallel-connected inverters," in *2018 International Power Electronics Conference (IPEC-Niigata 2018 -ECCE Asia)*, May 2018, pp. 2668–2672, doi: 10.23919/IPEC.2018.8507446.

[14] A. M. Diab, F. Guo, S. S. Yeoh, S. Bozhko, C. Gerada, and M. Galea, "Comparative stability analysis of synchronous reference frame current controllers operated at high fundamental frequency," *IEEE Transactions on Transportation Electrification*, vol. 9, no. 2, pp. 2115–2128, Jun. 2023, doi: 10.1109/TTE.2022.3208825.

[15] D. Ramasubramanian and E. Farantatos, "Viability of synchronous reference frame phase locked loop inverter control in an all inverter grid," in *2020 IEEE Power & Energy Society General Meeting (PESGM)*, 2020, doi: 10.1109/PESGM41954.2020.9282091.

[16] Z. Dai, G. Li, M. Fan, J. Huang, Y. Yang, and W. Hang, "Global stability analysis for synchronous reference frame phase-locked loops," *IEEE Transactions on Industrial Electronics*, vol. 69, no. 10, pp. 10182–10191, Oct. 2022, doi: 10.1109/TIE.2021.3125655.

[17] X. Ding, T. Lan, and H. Dong, "Control strategy and stability analysis of virtual synchronous generators combined with photovoltaic dynamic characteristics," *Journal of Power Electronics*, vol. 19, no. 5, pp. 1270–1277, 2019, doi: 10.6113/JPE.2019.19.5.1270.

[18] D. Jiawei, Z. Jiangbin, and M. Zihan, "VSG inertia and damping coefficient adaptive control," in *2020 Asia Energy and Electrical Engineering Symposium (AEEES)*, May 2020, pp. 431–435, doi: 10.1109/AEEES48850.2020.9121526.

[19] Q. Lin, T. Shijo, K. Ogawa, H. Uno, Y. Kanekiyo, and J. Arai, "Inertia evaluations on grid forming inverters with virtual synchronous generator control applied to photovoltaic power systems," in *2022 IEEE Energy Conversion Congress and Exposition (ECCE)*, Oct. 2022, pp. 1–6, doi: 10.1109/ECCE50734.2022.9947992.

[20] R. Shikuma, D. Orihara, H. Kikusato, H. Taoka, A. Kaneko, and Y. Hayashi, "Quantitative effect of the inertia emulation block of grid-forming inverters on frequency stability," in *2023 IEEE Belgrade PowerTech*, 2023, doi: 10.1109/PowerTech55446.2023.10202957.

[21] Q. Chen, B. Zhu, M. Liu, and S. Mao, "Analysis of grid-connected stability of VSG-controlled PV plant integrated with energy storage system and optimization of control parameters," *Electronics (Switzerland)*, vol. 13, no. 7, 2024, doi: 10.3390/electronics13071343.

[22] J. Gong, S. Li, W. Xia, and W. Liu, "A constrained optimal power flow algorithm for grid-connected power systems with small disturbance stability considering PV-VSG," in *2023 Power Electronics and Power System Conference (PEPSC)*, Nov. 2023, pp. 305–309, doi: 10.1109/PEPSC58749.2023.10395431.
[23] R. Pan and P. Sun, "Multifunctional inverter based on virtual synchronous machine implemented in synchronous reference frame," *Electrical Engineering*, vol. 103, no. 4, pp. 2093–2111, Aug. 2021, doi: 10.1007/s00202-021-01220-w.
[24] T. Hornik and Q.-C. Zhong, "Control of grid-connected DC-AC converters in distributed generation: Experimental comparison of different schemes," in *2009 Compatibility and Power Electronics*, May 2009, pp. 271–278, doi: 10.1109/CPE.2009.5156046.
[25] G. Cao, H. Wu, Y. Liu, and Q. Ren, "Distributed virtual inertia control strategy for multi-virtual synchronous machine parallel system based on neighbor communication," *Sensors*, vol. 25, no. 9, 2025, doi: 10.3390/s25092855.
[26] P. Utkarsha, N. K. S. Naidu, B. Sivaprasad, and K. A. Singh, "A flexible virtual inertia and damping control strategy for virtual synchronous generator for effective utilization of energy storage," *IEEE Access*, vol. 11, pp. 124068–124080, 2023, doi: 10.1109/ACCESS.2023.3330237.
[27] A. Fernández-Guillamón, E. Gómez-Lázaro, E. Muljadi, and Á. Molina-García, "Power systems with high renewable energy sources: A review of inertia and frequency control strategies over time," *Renewable and Sustainable Energy Reviews*, vol. 115, p. 109369, Nov. 2019, doi: 10.1016/j.rser.2019.109369.
[28] IEEE, "IEEE standard for interconnection and interoperability of distributed energy resources with associated electric power systems interfaces," *IEEE Std 1547-2018 (Revision of IEEE Std 1547-2003)*, no. February. IEEE, Piscataway, NJ, USA, pp. 1–138, Feb. 15, 2018, doi: 10.1109/IEEESTD.2018.8332112.
[29] IEEE, "IEEE recommended practice and requirements for harmonic control in electric power systems," *IEEE Std 519-2022 (Revision of IEEE Std 519-2014)*. pp. 1–213, 2022.
[30] International Electrotechnical Commission (IEC), *IEC 61727 - PV systems characteristics of the utility interface*. Switzerland: IEC, 2004.

BIOGRAPHIES OF AUTHORS

Abdallah El Ghaly received his bachelor's degree in electrical power and control program, M.S.E. degree, and Ph.D. degree in electrical power and machines program from Beirut Arab University in Beirut, Lebanon, in 2013, 2016, and 2022, respectively. Dr. El Ghaly worked as a senior electrical design engineer from 2013 to 2019, participating in the design of commercial, industrial, and residential buildings worldwide, particularly in the Gulf region. He began his academic career at the Beirut Arab University in 2019 as a full-time lecturer. He is a full-time assistant professor in the electrical power and machines program at the Electrical and Computer Engineering Department, Faculty of Engineering, at the Beirut Arab University. He also serves as a reviewer for international journals and is currently serving as an assistant dean for the Faculty of Engineering. His research interests include power quality, active power filters, power electronics, and renewable energy systems. He can be contacted at email: a.ghali@bau.edu.lb.

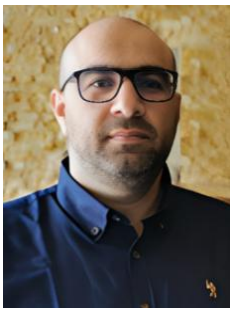

Abdullah Hamdan received his bachelor's degree in electrical power and machines from Beirut Arab University (BAU), Beirut, Lebanon, in 2010. He has more than a decade of professional experience with an international construction company, where he was involved in the execution and management of large-scale oil and gas facilities, infrastructure, power plants, and electrical substations. His expertise includes medium- and high-voltage electrical systems, construction and project management, and multidisciplinary coordination across projects in Turkmenistan, Mauritania, Oman, Kazakhstan, and Lebanon. In 2018, he completed management training programs at INSEAD and Korn Ferry (UAE), focusing on leadership, strategy, and organizational development. In 2024, he enrolled in the M.S.E. program in electrical power and machines at BAU, where his research focuses on "Stability Enhancement of Grid-Integrated Photovoltaic Systems: A Comparative Study," which is expected to be completed in December 2025. His research interests include photovoltaic systems, grid stability, and smart grids. He can be contacted at email: abdhamdane@gmail.com.

Mohamad Tarnini is a professor of electrical and computer engineering at Beirut Arab University (BAU), where he also serves as coordinator of the power and machines program. He has extensive teaching experience in the fields of power electronics, electric machines, and electric drives, and has supervised numerous undergraduate and postgraduate projects in these areas. His research interests include the modeling, analysis, and control of power electronic converters, harmonic mitigation techniques using active power filters, and the integration of renewable energy resources into modern power systems. He has published several papers in international journals and conferences, with a particular focus on photovoltaic (PV) systems, wind energy conversion technologies, and electric vehicle technologies. He is actively engaged in advancing sustainable power solutions and contributes to academic and professional communities through research collaborations, peer reviews, and program development. He can be contacted at email: m.tarnini@bau.edu.lb.